Energy loss mechanisms in the microdischarges in plasma display panels

Energy loss mechanisms in the microdischarges in plasma display panels

G. J. M. Hagelaar[a)]
Department of Physics, Eindhoven University of Technology, P.O. Box 513, 5600 MB Eindhoven, The Netherlands

M. H. Klein and R. J. M. M. Snijkers
Philips Research Laboratories Aachen, Weisshausstrasse 2, 52066 Aachen, Germany

G. M. W. Kroesen
Department of Physics, Eindhoven University of Technology, P.O. Box 513, 5600 MB Eindhoven, The Netherlands

(Received 23 August 2000; accepted for publication 8 November 2000)

Low luminous efficacy is one of the major drawbacks of plasma display panels (PDPs), where the main limiting factor is the efficiency of the microdischarges in generating UV radiation. In this work we use a two-dimensional self-consistent fluid model to analyze the energy loss mechanisms in neon–xenon discharges in coplanar-electrode color PDPs and interpret experimental data on the luminous efficacy of these PDPs. The modeling results are in good agreement with the measured UV emission spectrum and measured trends in the efficacy. Most of the electrical input energy is transferred to ions and subsequently to the gas and the surface. The electrical energy transferred to electrons is mostly used for ionization and excitation, where the part used for xenon excitation largely ends up in UV radiation. The amplitude, frequency, and rise time of the driving voltage mainly affect the energy losses due to ion heating. The xenon content also affects the conversion of electron energy into UV energy. © *2001 American Institute of Physics.*
[DOI: 10.1063/1.1337084]

I. INTRODUCTION

Plasma display panel (PDP) technology is a promising technology for large, lightweight, flat displays.[1,2] In PDPs, the light of each picture element (pixel) is emitted from a tiny high-pressure glow discharge, typically called a microdischarge. Color PDPs use microdischarges in xenon mixtures to generate UV radiation, and convert this into red, blue, and green light by phosphors. One of the major drawbacks of PDPs is their low luminous efficacy: about 1 lm/W, compared to 4 lm/W for the conventional cathode ray tube (CRT) displays.

In color PDPs, energy loss occurs in various ways: Only about 40% of the UV photons emitted by the discharges is captured by the phosphors, where an additional 80% of photon energy is lost in the conversion to visible light, mainly due to the difference in wavelength of the visible light (~600 nm) and the UV radiation (~150 nm). Next, only about half of the visible light emitted by the phosphors leaves the display on the front side, the other half is absorbed somewhere in the display. However, the largest energy loss occurs in the microdischarges themselves: only about 10% of the electrical input energy is used for the emission of UV photons. In this article, we use a two-dimensional self-consistent fluid model[3] to analyze the energy loss mechanisms in the microdischarges and interpret experimental data on the luminous efficacy. We extend, improve, and discuss more elaborately the analysis briefly presented in Refs. 4 and 5.

We consider the most common type of color PDP: the coplanar-electrode ac PDP.[6] Figure 1 schematically depicts a PDP of this type. The panel consists of two glass plates, separated by a gap of about 150 μm that is filled with a mixture of neon and a small percentage of xenon at 450 Torr. Each plate is equipped with a large number of parallel electrodes, covered by dielectric material. A discharge cell (corresponding to a pixel) is formed by the intersection of a pair of sustain electrodes on the front plate, and an address electrode on the back plate. In operation, a square wave voltage with a frequency of 50–250 kHz is constantly applied between each pair of sustain electrodes. The amplitude of this sustain voltage is below the breakdown voltage. To switch a certain discharge cell on, a write voltage pulse is applied between the address electrode and one of the sustain electrodes of the cell. This initiates a microdischarge, which is quickly quenched due to the accumulation of surface charge on the dielectric material that covers the electrodes. On its next half cycle, the sustain voltage changes polarity. The stored surface charge now reinforces the sustain voltage, causing the ignition of a new microdischarge, despite the fact that the sustain voltage itself is below the breakdown voltage. A new surface charge distribution develops, quenches the discharge again, and so on. In this way, a transient microdischarge occurs in the cell every time the sustain voltage changes polarity, due to the presence of surface charge.

The article is organized as follows: Secs. II and III outline the fluid model and the simulation of the transient microdischarges in a PDP cell. In Sec. IV we analyze how the electrical energy is dissipated in the discharge. In Sec. V we study how the energy dissipation and the resulting discharge

a)Electronic mail: hagelaar@discharge.phys.tue.ni

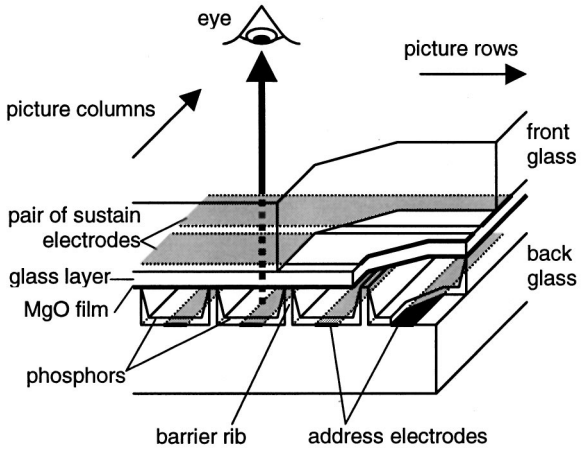

FIG. 1. Schematic drawing of a coplanar-electrode ac PDP.

efficiency are influenced by several discharge parameters, thus interpreting measured trends in the luminous efficacy.

II. DESCRIPTION OF THE MODEL

To simulate the PDP discharges we use the two-dimensional model presented in Ref. 3. Following the well-known fluid approach, this model describes the behavior of plasma particle species (electrons, ions, and excited neutrals) by the first few moments of the Boltzmann equation: the continuity equation, the momentum transport equation, and the energy transport equation. For each plasma particle species p the evolution of the number density n_p is calculated from a continuity equation

$$\frac{\partial n_p}{\partial t}+\nabla\cdot\Gamma_p=\sum_r c_{p,r}R_r, \tag{1}$$

where Γ_p is the particle flux, and the right hand side represents the total particle production or loss in reactions. The summation is over all possible reactions r, where R_r is the reaction rate and $c_{p,r}$ is the net number (positive or negative) of particles of species p created in one reaction of type r. The flux is given by the momentum transport equation, which we approximate by the drift-diffusion equation

$$\Gamma_p=\mathrm{sgn}(q_p)\mu_p\mathbf{E}n_p-D_p\nabla n_p. \tag{2}$$

Here $\mathbf{E}$ is the electric field, q_p is the particle charge, μ_p is the mobility and D_p is the diffusion coefficient. The first term represents the flux due to the electric field (drift), the second term the flux due to concentration gradients (diffusion). Particle inertia is neglected. The electric field is self-consistently calculated from Poisson's equation

$$\nabla\cdot(\varepsilon\mathbf{E})=\sum_p q_p n_p, \tag{3}$$

where ε is the dielectric permittivity.

Equations (1) and (2) require the input of mobilities, diffusion coefficients, and reaction rate coefficients. In general these quantities depend on the energy distribution of the considered particles. For ions we use the local field approximation, which assumes a direct relation between the particle energy distribution and the local electric field: the ion diffusion coefficients and mobilities are regarded as functions of the electric field. For the electrons however, the local field approximation seems unrealistic, in view of the combination of the poor energy transfer in electron-neutral collisions and the strong spatial variations of the electric field in PDP discharges. Unlike most PDP models,[7–11] our model does not adopt the local field approximation for electrons, but assumes the electron mobility, electron diffusion coefficient, and the rate coefficients of electron impact reactions to be functions of the electron mean energy. The electron mean energy $\overline{\varepsilon}$ is calculated from the energy balance equation

$$\frac{\partial(n_e\overline{\varepsilon})}{\partial t}+\nabla\cdot\left(-\frac{5}{3}\mu_e\mathbf{E}(n_e\overline{\varepsilon})-\frac{5}{3}D_e\nabla(n_e\overline{\varepsilon})\right)$$
$$=-e\Gamma_e\cdot\mathbf{E}-\sum_r\overline{\varepsilon_r}R_r, \tag{4}$$

where n_e is the electron density, μ_e is the electron mobility, D_e is the electron diffusion coefficient, and Γ_e is the electron flux. The two terms on the right-hand side represent heating by the electric field and energy loss in collisions, respectively. The summation in the loss term is only over the electron impact reactions, with $\overline{\varepsilon_r}$ the threshold energy. Energy loss due to elastic collisions is included in this term by using an imaginary threshold energy of 1 eV in combination with an effective collision rate. Contrary to Ref. 12, we found that

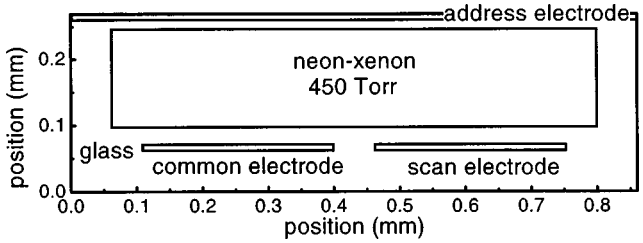

FIG. 2. Model geometry used in the calculations. This geometry represents a discharge cell of a coplanar-electrode PDP. The top of the geometry corresponds to the back plate of the display, the bottom to the front plate. The sustain electrodes are indicated as the common and scan electrodes. The dielectric constant of the glass is 11.0.

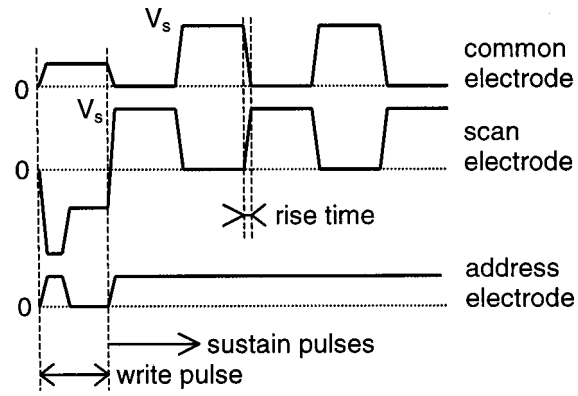

FIG. 3. Electrode potentials as a function of time in the model driving scheme. This figure relates to the model geometry shown in Fig. 2, where the common and scan electrodes are the sustain electrodes. Typically the amplitude of the sustain voltage is $V_s=180-300$ V, its frequency 50–250 kHz.

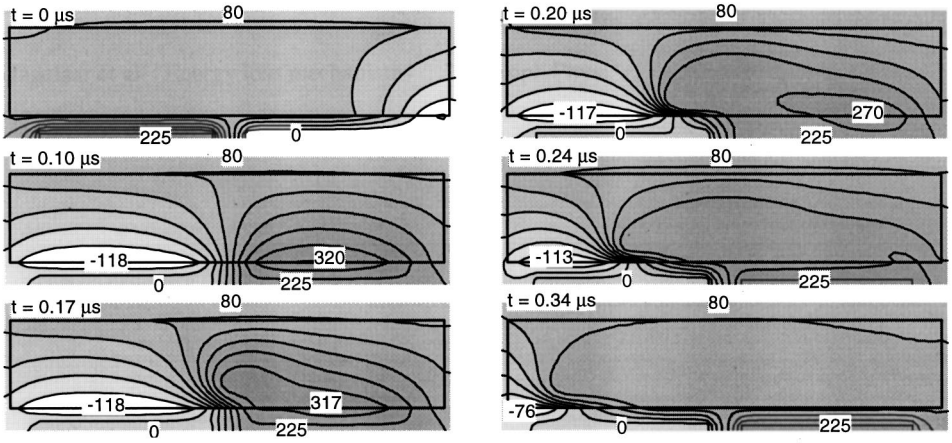

FIG. 4. Time evolution of the electric potential profile during a PDP discharge. The geometry is shown in Fig. 2. The sustain voltage is 225 V, the sustain frequency is 50 kHz, the pressure is 450 Torr, and the xenon percentage is 5%. The moment $t=0$ corresponds to the end of the previous sustain pulse; the sustain voltage is switched between $t=0$ μs and $t=0.10$ μs, with a rise time of 0.10 μs. The increment of the contours is 1/10 times the difference of the maximum and minimum values, which are indicated in each plot. The unit of the indicated potentials is V.

the electron energy equation considerably improves the reliability of the PDP model; for the calculated discharge efficiency the difference with the local field approximation may be as large as a factor of two.

The transport Eqs. (1) and (2) for heavy species are solved for the boundary condition of zero particle reflection and influx. The boundary conditions for the electron equations are similar, but include an influx by secondary electron emission. Poisson's equation is solved not only in the discharge, but also in surrounding dielectric materials, taking into account possible surface charge. For details on the basic equations and the boundary conditions we refer to Ref. 3.

The considered model geometry, shown in Fig. 2, represents a discharge cell, or actually an entire row, of the display. Due to its two dimensionality, the model geometry is only an approximation of the real PDP geometry, which has important three-dimensional features. The barrier ribs that separate the columns of the display are not represented in the model; instead, the model cell has side walls along the sustain electrodes. (Compare Fig. 2 with Fig. 1.) The model electrode driving scheme is shown in Fig. 3. Although each simulation is started with a write pulse to initiate the discharges and switch the cell on, we will not consider the writing itself in this article. An external circuit, involving backcoupling from the current to the electrode voltage, is not included in the model. We do however take into account a realistic rise time ($\sim$100 ns) for all voltage changes. We remark that in the model the required sustain voltages are generally slightly higher (20%) than in reality. This difference can easily be removed by adjusting the model input data (e.g., the secondary emission coefficients) within their experimental inaccuracies, but in our opinion such adjustments are unnecessary and might even be deceiving. The electrical behavior of the discharge and the mechanisms of UV photon generation are described by an extensive reaction scheme, similar to the scheme used in Ref. 7, consisting of 80 reactions, involving 15 different plasma species. The full simulation of a single PDP discharge takes 15–20 min on a modern personal computer.

III. SIMULATION OF A PDP DISCHARGE

Figures 4 and 5 show the electric potential and the xenon excitation rate in the model geometry, during the simulation of a typical PDP discharge. By the end of the discharge that precedes the one considered in these figures, stored surface charge screens the discharge gas almost entirely from the applied voltage. After the sustain voltage has been switched, the same surface charge reinforces the applied voltage rather than canceling it. The total voltage across the discharge gas is now so high that the ignition of a new discharge takes place. It appears from Figs. 4 and 5 that the discharge starts in the center of the geometry, where the electrodes are close together. As soon as a new surface charge distribution is established in the center of the geometry, the discharge spreads outward. Eventually, all the electrodes are screened by the new surface charge distribution, and the discharge stops. Note that the current through the electrodes is a displacement current resulting from the changes in the electric fields in the dielectric layer that covers them. During the discharge extremely strong electric fields are present in the

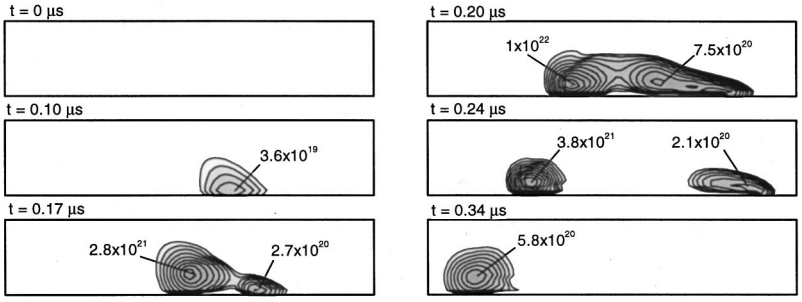

FIG. 5. Time evolution of the excitation rate of the resonant $Xe^*(^3P_1)$ state during a PDP discharge. This figure shows results of the same simulation as Fig. 4; the discharge conditions are indicated in the caption of that figure. For all plots the contours correspond to a logarithmic scale covering the range from 10^{18} to 10^{22} cm^{-3} s^{-1}; the increment of the contours is a factor of 2.51. The unit of the values indicated in the plots is cm^{-3} s^{-1}.

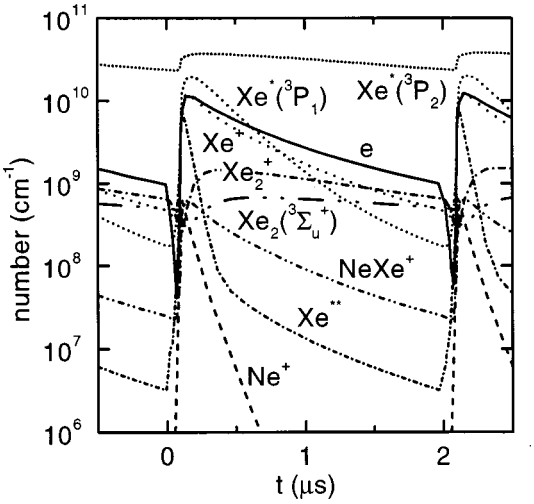

FIG. 6. Time evolution of the numbers of particles of the most important species. This figure shows results of the same simulation as Fig. 4; the discharge conditions are indicated in the caption of that figure.

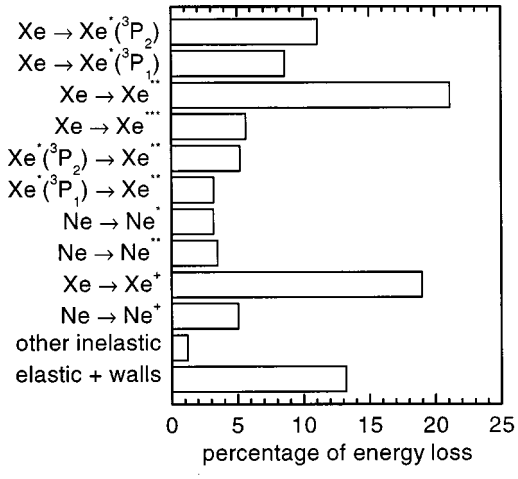

FIG. 8. Breakdown of the loss of electron energy into the different electron impact excitation and ionization processes. The discharge conditions are indicated in the caption of Fig. 7.

plasma sheath front of the cathode, which has the character of a cathode fall. Ionization and excitation mainly take place in the vicinity of this cathode sheath.

Figure 6 shows the calculated time evolution of the (space integrated) densities of the most important species during the discharge. The densities rapidly increase at the beginning of the sustain pulse and then gradually decay. Neon ions are only present during the very first part of the discharge; during the plasma decay Xe_2^+ becomes the most important ion species.

IV. ANALYSIS OF THE ENERGY DISSIPATION

During the discharge electrical energy is transferred to the plasma through the acceleration of the charged particles. The energy that is thus consumed by the particle species p is

$$W_p = \int_{\text{time}} \int\int\int_{\substack{\text{discharge}\\ \text{volume}}} q_p \Gamma_p \cdot \mathbf{E} d^3V dt. \tag{5}$$

Note that the sum of these energies must be equal to the total electrical energy input:

$$\sum_p W_p = \int_{\text{time}} I \times V dt, \tag{6}$$

where I is the (displacement) current through a sustain electrode and V is the sustain voltage. We confirmed that this relation is reproduced by the fluid model within 0.01%, which illustrates its numerical consistency. The main energy consumption takes place in the plasma sheaths, mostly on the cathode side of the discharge, where the sheath contains an extremely strong electric field, as can be seen in Fig. 4.

Figure 7 shows the calculated energy consumption of the various charged particle species in a typical PDP discharge. The larger part of the energy turns out to be consumed by ions. This energy is forever lost for the production of UV photons: under PDP discharge conditions ionization or excitation by ion impact seem negligible, which implies that all the ion energy is eventually transferred to the gas and the surface. We remark that ion impact ionization or excitation is not included in the model; even if they would occur, we

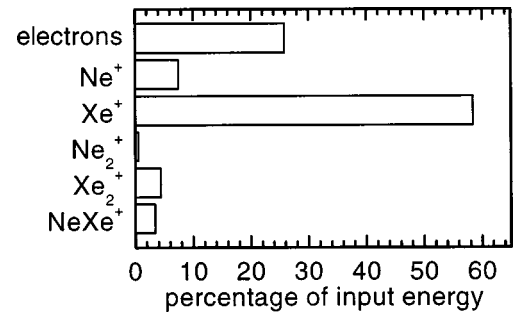

FIG. 7. Breakdown of the electrical input energy into the heating of the different charged particle species. The total energy consumption is 3.4 $\times 10^{-7}$ J per discharge (pulse) per cm^{-1} of row length. The sustain voltage is 225 V, the sustain frequency is 250 kHz, the gas pressure is 450 Torr, and the xenon percentage is 5%.

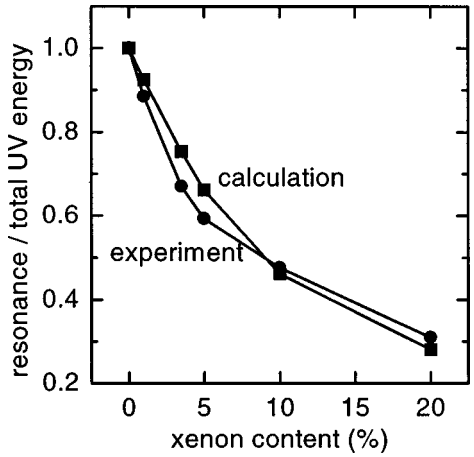

FIG. 9. Ratio of the energy carried by 147 nm resonance photons and the total energy carried by UV photons. This plot compares the result of fluid simulations to the experimental data of Ref. 13. The discharge conditions, for both simulation and experiment, are the same as with Fig. 7. The experimental discharge geometry is very similar to the model geometry of Fig. 2.

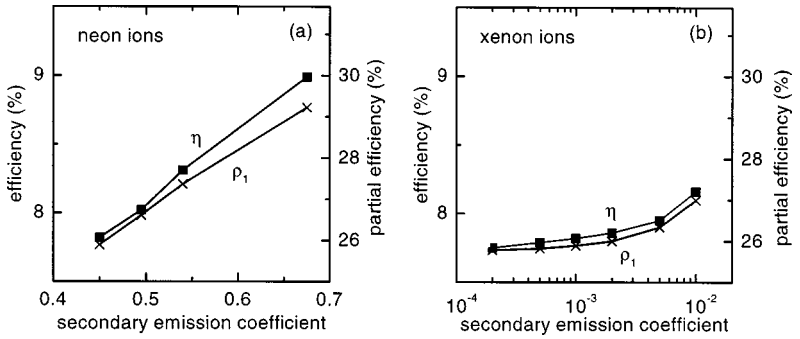

FIG. 10. Calculated efficiency as a function of the secondary emission coefficient, for (a) neon ions and (b) xenon ions. The sustain voltage is 225 V, the sustain frequency is 250 kHz, the xenon percentage is 5%.

would not see them in the simulations. The electron energy, on the other hand, is largely used for the excitation and ionization. The energy that is used for a reaction r is

$$W_r = \int_{\text{time}} \int_{\substack{\text{discharge} \\ \text{volume}}} \overline{\varepsilon_r} R_r d^3V dt. \tag{7}$$

Figure 8 shows how the electron energy is used in the different reactions. Note that the electron energy Eq. (4) ensures that the sum of all the energy losses in Fig. 8 is equal to the total energy transferred to electrons by the field as given by Eq. (5).

Of all the processes in Fig. 8 it is mainly the excitation of xenon atoms that eventually leads to the generation of UV photons. There are several possible mechanisms: First, the resonant state $Xe^*(^3P_1)$ decays directly to the ground state, emitting UV photons at a wavelength of 147 nm. Second, both the resonant $Xe^*(^3P_1)$ and metastable $Xe^*(^3P_2)$ states may attach to xenon gas atoms and form excited dimers Xe_2^*; these dimers decay radiatively into ground state atoms. The photons thus emitted by the higher vibrational levels $Xe_2^*(O_u^+)$ are distributed around 150 nm, those emitted by the lower vibrational levels $Xe_2^*(^3\Sigma_u^+, ^1\Sigma_u^+)$ around 173 nm. The higher atomic states Xe** and Xe*** do not directly lead to UV photons, but cascade down to the $Xe(^3P_1, ^3P_2)$ levels. In this case some amount of energy is lost in the form of infrared radiation or gas heating.

The energy that is emitted from the discharge in the form of UV photons with a wavelength λ is

$$W_\lambda = \int_{\text{time}} \int_{\substack{\text{discharge} \\ \text{volume}}} (hc/\lambda) R_\lambda d^3V dt, \tag{8}$$

where h is Planck's constant, c is the velocity of light, and R_λ is the rate of the decay process leading to the emission. The relative importance of the different UV wavelengths (147, 150, and 173 nm) depends heavily on partial xenon pressure. Figure 9 shows the fraction of the UV energy emitted at 147 nm, $W_{147\,\text{nm}}/(W_{147\,\text{nm}}+W_{150\,\text{nm}}+W_{172\,\text{nm}})$, as a function of the xenon content. The simulation results are in excellent agreement with the experimental values of Ref. 13, determined by integrating the measured emission spectrum.

V. PARAMETRIC STUDIES

The efficiency of the discharge in generating UV photons is defined as

$$\eta = \sum_\lambda W_\lambda \Big/ \sum_p W_p. \tag{9}$$

In view of the analysis given in the previous section, it is interesting to split the discharge efficiency into two partial efficiencies

$$\rho_1 = W_e \Big/ \sum_p W_p, \tag{10}$$

$$\rho_2 = \sum_\lambda W_\lambda \Big/ W_e, \tag{11}$$

where W_e is the electrical energy transferred to the electrons, as given by Eq. (5) and $\eta = \rho_1 \rho_2$. The partial efficiency ρ_1 is the efficiency of the discharge in heating the electrons, ρ_2 is the efficiency of the electrons in generating UV radiation.

We will now investigate how the η, ρ_1, and ρ_2 are influenced by various discharge parameters. Wherever possible, we will compare the simulation results with experi-

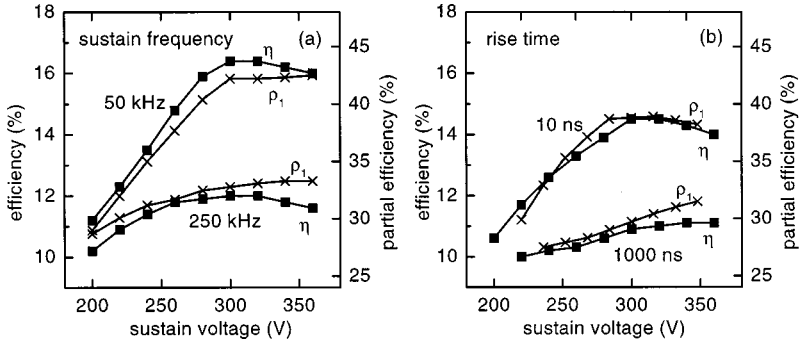

FIG. 11. Calculated efficiency as a function of the sustain voltage, for (a) two different frequencies and a rise time of 100 ns, and (b) two different rise times and a frequency of 250 kHz. The xenon percentage is 5%.

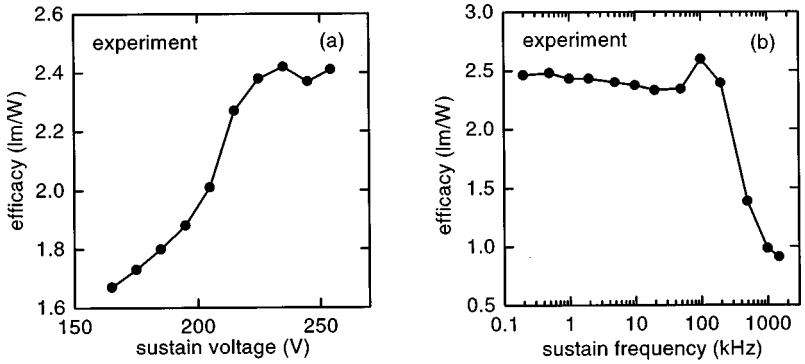

FIG. 12. Measured efficacy as a function of (a) the sustain voltage, where the frequency is 250 kHz, and (b) the sustain frequency, where the voltage is 225 V (Ref. 12). The xenon percentage is 10%.

mental data on the PDP efficacy of 4 in. test panels, taken from Ref. 14. The efficacy is a measure for the light output of the display—weighted according to the sensitivity of the human vision—per unit of electrical input energy; it is thus not only determined by the discharge efficiency, but also by other factors, such as the efficiency of the phosphors in converting the UV radiation into visible light. Here we assume that these other factors stay constant. The experimental electrode size and distance, thickness of the covering dielectric layer, and cell height are well reflected by the model geometry of Fig. 2.

We start with the influence of the secondary emission coefficient. In present day PDPs, where the surface is coated with magnesium oxide, this coefficient has been estimated to be around 0.45 for neon ions and below 0.001 for xenon ions.[15] Figure 10 shows that both η and ρ_1 increase with increasing secondary emission coefficient; ρ_2 is nearly unaffected. This result is not very surprising: The secondary emission coefficient directly determines the relative contributions of the electrons and the ions to the current density in the cathode fall, where the main particle heating occurs. The relative contribution of the electrons—and consequently ρ_1—increases monotonically with increasing secondary emission coefficient. Of main importance is the secondary emission coefficient of the neon ions. For xenon ions, the secondary emission coefficient is so low that its exact value does not really matter: xenon hardly contributes to the secondary emission anyway.

The effect of the sustain voltage is shown in Fig. 11. For not too high sustain voltages, both η and ρ_1 increase with increasing voltage. This trend is also seen in the efficacy measurements shown in Fig. 12(a). The model reveals the mechanism behind this trend: As the voltage increases, the electric fields and the electron energies in the discharge go up. Since neon has a higher ionization energy than xenon, this leads to an increase of the relative contribution of neon to the total ion flux, which implies an increase of the average secondary emission coefficient. As we have seen before, this is favorable for the electron heating efficiency ρ_1.

Figure 11(a) also shows that the sustain frequency has a strong effect on the calculated efficiency. This fact is known from experiments; see Fig. 12(b): Beyond a certain sustain frequency, the discharge efficiency drops dramatically. In Refs. 4 and 5 it is suggested that this effect is caused by the role played by metastable xenon atoms. However, when looking at the modeling results more carefully, we find an entirely different underlying mechanism: At low frequencies (50 kHz) there is a short time between the switching of the sustain voltage and the breakdown. At high frequencies (250 kHz), the plasma does not completely decay in between the discharges, which facilitates their ignition: breakdown now already occurs during the switching of the voltage. This is illustrated by Fig. 13. Due to the premature breakdown, the surface charge on the dielectric layer is already changed before the sustain voltage reaches its full value, so that the final voltage across the gas is lower. As we have seen before, this results in a lower ρ_1. This observation suggests that for high frequencies (250 kHz) the rise time of the sustain voltage might influence the efficiency. According to the simulation results shown in Fig. 11(b) this is indeed the case. For 50 kHz no influence of the rise time is found: rise times of 10, 100, and 1000 μs yield exactly the same efficiency [not shown in Fig. 11(b)]. We remark that these results are only of qualitative value. In general, the exact time between the switching of the voltage and the breakdown is not very accurately predicted by fluid models.[8]

As we have seen, the amplitude, frequency, and rise time of the sustain voltage mainly affect η via ρ_1, leaving ρ_2 nearly unchanged. A parameter that can be expected to directly affect ρ_2 is the xenon content of the gas mixture. Fig-

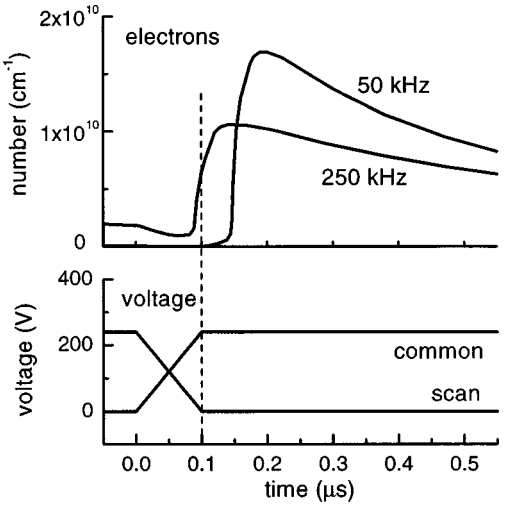

FIG. 13. Comparison between of the time evolution of the electron density for two different sustain frequencies. The xenon percentage is 5%.

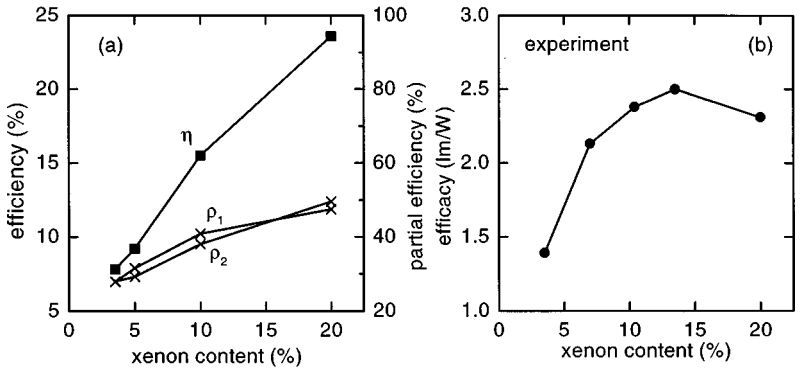

FIG. 14. Influence of the percentage of xenon on (a) the calculated efficiency and (b) the measured efficacy (Ref. 12). In both the simulation and the experiment the sustain frequency is 250 kHz. The sustain voltage is 260 V in the simulation and 225 V in the experiment.

ure 14(a) shows that the calculated efficiency increases with increasing percentage of xenon. This trend has been reported in the literature, e.g., in Ref. 7, but is not fully reflected by the efficacy measurements shown in Fig. 14(b). We remark that it is known that the phosphor performance strongly depends on the UV wavelength, which is influenced as well by the xenon percentage (see Fig. 9). It appears from Fig. 14(a) that not only ρ_2, but also ρ_1 is responsible for the increase of η with increasing xenon content.

VI. CONCLUSIONS

The fluid model presented in Ref. 3 is capable of simulating the microdischarges in a coplanar-electrode PDP. We have reproduced a write pulse and a series of sustain pulses in one cell of the display.

From the simulation results, we have analyzed how the electrical input energy is dissipated in the cell. The largest part of the electrical energy is transferred to ions and subsequently to the gas and the surface. The electrical energy transferred to electrons is mostly used for ionization and excitation. The part used for xenon excitation largely ends up in UV radiation. The calculated fraction of the UV energy that is carried by resonance photons is in excellent agreement with experimental results.

We have studied how the energy loss mechanisms are influenced by several discharge parameters. The amplitude, frequency, and rise time of the sustain voltage mainly affect the losses due to ion heating. The xenon content also affects the conversion of electron energy into UV energy. The trends in the calculated discharge efficiency are in good agreement with measured trends in the luminous efficacy.

ACKNOWLEDGMENTS

This work was supported by the Philips Research Laboratories in Eindhoven, The Netherlands. The authors thank G. Oversluizen and S. de Swart of these laboratories for the experimental data on the luminous efficacy.

[1] L. Weber, in *Flat-Panel Displays and CRTs*, edited by L. Tannas (Van Nostrand Reinhold, New York, 1985), pp. 332–407.
[2] A. Sobel, IEEE Trans. Plasma Sci. **19**, 1032 (1991).
[3] G. J. M. Hagelaar, G. M. W. Kroesen, U. van Slooten, and H. Schreuders, J. Appl. Phys. **88**, 2252 (2000).
[4] M. Klein, R. Snijkers, and G. Hagelaar, *Proceedings of the 6th International Display Workshop* (Society for Information Display, Japan, 1999), pp. 695–698.
[5] M. H. Klein, R. J. M. M. Snijkers, and G. J. M. Hagelaar, IEICE Transactions *E83-C*, 1602 (Institute of Electronic, Information and Commincation Engineers, 2000).
[6] H. Hirakawa *et al.*, SID Digest 279 (Society for information Display, 1998).
[7] J. Meunier, Ph. Belenguer, and J. P. Boeuf, J. Appl. Phys. **78**, 731 (1995).
[8] C. Punset, J.-P. Boeuf, and L. C. Pitchford, J. Appl. Phys. **83**, 1884 (1998).
[9] R. Veerasingam, R. B. Campbell, and R. T. McGrath, IEEE Trans. Plasma Sci. **23**, 688 (1995).
[10] R. Veerasingam, R. B. Campbell, and R. T. McGrath, IEEE Trans. Plasma Sci. **24**, 1411 (1996).
[11] S. Rauf and M. J. Kushner, J. Appl. Phys. **85**, 3470 (1999).
[12] S. Rauf and M. J. Kushner, J. Appl. Phys. **85**, 3460 (1999).
[13] R. Snijkers and M. Klein, *52nd Gaseous Electronics Conference*, Norfolk, Virginia, 5–8 October 1999.
[14] G. Oversluizen and S. de Zwart (private communication).
[15] C. Punset, Th. Callegari, and J.-P. Boeuf, *Proceedings of the International Symposium on Future Emissive Displays*, Tottori University, Tottori, Japan, 10–11 December 1998, pp. 87–93.